

Impacts of suspended clay particle deposition on sand-bed morphodynamics

J. Dallmann¹, C. B. Phillips², Y. Teitelbaum³, N. Sund⁴, R. Schumer⁴, S.

Arnon³, A. I. Packman²

¹Department Mechanical Engineering, Northwestern University, Evanston, IL, USA

²Department of Civil and Environmental Engineering, Northwestern University, Evanston, IL, USA

³Zuckerberg Institute for Water Research, The J. Blaustein Institutes for Desert Research, Ben-Gurion

University of the Negev, Beersheba, Israel

⁴Desert Research Institute, Reno, Nevada, USA

Key Points:

10

11

12

13

14

15

- Initially suspended fine clay particles within the water column rapidly accumulate within the sediment bed due to hyporheic exchange
- Fine clay particle storage occurs beneath the mobile layer of the sediment bed defined by the extent of bedform scour
- Formation of the fine particle layer results in reductions of bedform celerity, height and sediment flux while length is unchanged

Corresponding author: J.Dallmann, jonathandallmann2020@u.northwestern.edu

This article has been accepted for publication and undergone full peer review but has not been through the copyediting, typesetting, pagination and proofreading process which may lead to differences between this version and the Version of Record. Please cite this article as doi: 10.1029/2019WR027010

Abstract

17

18

20

21

22

23

25

26

27

29

31

32

33

35

36

37

30

40

41

42

43

44

46

48

Fine particles (0.1-100 microns) are ubiquitous within the water column. Observations on the interactions between suspended fine particles and sediment beds remain limited, reducing our ability to understand the interactions and feedbacks between fine particles, morphodynamics and hyporheic flow. We performed laboratory experiments to explore changes in bedform morphodynamics and hyporheic flow following the progressive addition of kaolinite clay to the water column above a mobile sand bed. We characterized these interactions by taking high-frequency time series measurements of bed topography and freestream clay concentration combined with solute injections and bed sediment cores to characterize subsurface properties. Deposition of initially suspended clay resulted in a decrease of bedform height, celerity and sediment flux by 14%, 22% and 29% when 1000g was accumulated within the bed (equal to clay/sand mass ratio of 0.4% in the bed). The hyporheic exchange flux decreased by almost a factor of 2 for all clay additions, regardless of the amount of clay eventually deposited in the bed. Post experiment sediment cores showed clay accumulation within and below the mobile layer of the bedforms, with the peak concentration occurring at the most frequent bedform scour depth. These results demonstrate the tight coupling between bed sediment morphodynamics, fine particle (clay) deposition, and hyporheic exchange. Suspended and bed load transport rates are diminished by the transfer of suspended load to the sediment via hyporheic exchange. This coupling should be considered when estimating sediment transport rates.

1 Introduction

In rivers, fine particles with a diameter of <100 microns consist of particulate organic carbon, minerals such as clay, algal and bacterial cells, and other contaminants (Drummond, Aubeneau, & Packman, 2014; Drummond, Larsen, Gonzalez-Pinzon, Packman, & Harvey, 2018). Natural sources of these fine particles include induced overland flow and erosion, remobilization of fine particles stored in the stream bed, bank erosion, landslides and other mass failures (Belmont et al., 2011; Mueller & Pitlick, 2013; Owens et al., 2005; Rose, Karwan, & Godsey, 2018; Sekely, Mulla, & Bauer, 2002). Anthropogenic activity, such as mining, agriculture, logging, and urbanization can increase fines within rivers (Karwan, Aalto, Aufdenkampe, Denis Newbold, & Pizzuto, 2011; Nelson & Booth, 2002; Vaughan, Belmont, Hawkins, & Wilcock, 2017; Wolman, 1967; Wood & Armitage, 1997). Fine particles represent a significant water quality concern (Bilotta & Brazier,

2008) with harmful effects including increased turbidity in pristine waters (Lloyd, Koenings, & Laperriere, 1987), decreasing stream productivity (Ryan, 1991), damage to benthic ecological systems (Owens et al., 2005), and hypoxia in coastal systems due to excess nutrients (Ansari, 2005; Paerl & Otten, 2013). In addition, the fate of contaminants are linked to the dynamics of fine particles (Foster & Charlesworth, 1996; Horowitz, 2009; Zhang et al., 2010).

49

50

52

56

57

61

63

65

70

71

72

73

74

75

76

77

79

80

81

The flow of water into and out of the stream bed (hyporheic exchange), fine particle transport and deposition are tightly coupled in river systems (Boano et al., 2014; Harvey et al., 2012; Karwan & Saiers, 2012; Packman & Mackay, 2003). In the presence of fine particles, hyporheic exchange leads to deposition and filtration of fine particles due to advective pumping and turbulent exchange with the stream bed (Boano et al., 2014; Packman, Brooks, & Morgan, 2000b, 2000a). The accumulation of fines in the bed via filtration, in turn, leads to decreasing hyporheic exchange (Fox, Packman, Boano, Phillips, & Arnon, 2018; Packman & Mackay, 2003). These fines may be stored there for long periods of time spanning multiple flood events (Drummond et al., 2014; Harvey et al., 2012). Through their role in setting the storage and release times of fine particles, hyporheic exchange and bed sediment transport are important for understanding the long-term fate of contaminants and waterborne pathogens (Boano et al., 2014; Drummond et al., 2014). Excessive deposition of fines results in the siltation (colmation) of stream beds reducing the transfer of various solutes and particles such as organic carbon and regulating heat transfer (Hartwig & Borchardt, 2015). Siltation is expected to impact the microbial biomass residing within the upper sediment bed (Merill & Tonjes, 2014), and harm the spawning potential of diadromous fish (Chapman, 1988; Greig, Sear, & Carling, 2005; Louhi, Ovaska, Maki Petays, Erkinaro, & Muotka, 2011). Reduction in hyporheic exchange negatively impacts these communities, leading to increased in-stream nutrient content (Feris et al., 2003, 2004; Li, Aubeneau, Bolster, Tank, & Packman, 2017).

Clay and fine particles are prevalent across many fluvial and marine systems from coarse grained mountain streams to estuarine and shallow marine systems. Coupled fine particle and bed morphodynamic interactions are expected to occur in sand bedded rivers, estuaries, near coastal environments, and shallow marine settings. The presence of stationary sand bedforms, such as dunes and ripples, have been shown to greatly increase hyporheic exchange compared to a featureless bed (Elliot & Brooks, 1997; Fox et al., 2018; Packman & Mackay, 2003; Thibodeaux & Boyle, 1987). The addition of active bed sed-

inent transport remains under studied, though mobile bedforms are known to change hyporheic exchange pathways and reduce the rate of nitrogen removal relative to stationary ones (??) as mobile bedforms alter the patterns of fine particle deposition and remobilization (Boano et al., 2014; Packman, Brooks, & Morgan, 2001; Phillips, Dallmann, Jerolmack, & Packman, 2019), understanding how exchange is impacted by sediment transport is necessary for modeling the fate of fine particles in natural systems where mobile bed conditions are common (e.g. floods). For stationary bedforms even relatively small amounts of fine particles can disrupt hyporheic exchange (Fox et al., 2018; Packman et al., 2000b, 2000a). However, mobile bedforms disrupt the surface clogging layers that develops in stationary beds, leading to no impact on hyporheic exchange with small fine particle additions and lower flow rates (Rehg, Packman, & Ren, 2005). It remains unclear though how this process will be impacted under higher concentrations of fine particles, or for sustained background concentrations of fines.

High concentrations of suspended fine particles have been observed to impact bed morphodynamics due to modulation of the stream turbulence. Both river field measurements (Smith & McLean, 1977) and laboratory experiments (Wan, 1984) show that the height to wavelength ratio for sandy bedforms tend to become smaller in the presence of large concentrations of suspended clay. Experiments on mixed clay and sand beds and premixed clay and sand slurries reveal complex feedback mechanisms between clay concentration, bedform morphodynamics, and flow structure (Baas & Best, 2002, 2008; Best, 2005). In particular, the turbulent characteristics of the flow are impacted by higher clay concentrations (conc. > 4 g/L), leading to morphodynamic changes (Baas & Best, 2008). This increased turbulence leads to an increase in both bedform height and wavelength for increasing freestream clay concentration (Baas, Best, & Peakall, 2011). However, in the more cohesive beds (clay percentage > 13%), winnowing of clay particles produced a segregated bed composed of a mobile sand layer above a mixed clay/sand bed (Baas, Davies, & Malarkey, 2013).

Though the impact of clay on bed morphodynamics under premixed conditions have been well studied, it remains unclear how deposition and accumulation of suspended fine particles may impact sand bed morphodynamics. This mode of interaction is especially relevant in rivers and estuaries, where the introduction of clay and other fine particles is episodic in nature, often co-varying with higher flows due to runoff generated during storms. Further, the ecological implications of the human-induced increases in fine par-

ticles to rivers can only be inferred without an understanding of how fine particles (clay) introduced to rivers from their catchment may impact bed morphodynamics and hyporheic exchange. This study uses four experiments to explore the role of clay concentration within the water column on mobile bedforms, clay accumulation within the bed, and hyporheic exchange.

2 Methods

2.1 Experimental Methods

We performed four experimental runs for a constant freestream velocity consisting of episodic injections of kaolinite clay leading to water suspensions of varying concentrations. The experiments differed only in the total amount of clay added to the flume and the sequence (i.e. number) of clay injections. The experiments were conducted using an 8.5 m long by 0.2 m wide tilting recirculating flume, equipped with a pump (Baldor Industrial Motors) that recirculated both water and sediment from the endwell (Figure 1a). Each experiment initially consisted of an initially flat clay free mobile sand bed approximately 10 cm thick - 250 kg of Flint Silica 12 (US Silica, Ottawa, IL) with a D_{50} of 0.420 mm given by the manufacturer - under a constant flow. Mean freestream height (15 cm), mean velocity (0.43 m/s) and shear velocity ($u^* = 0.026$ m/s) were the same for all experiments. The u^* was determined by fitting a log law velocity profile to a time-averaged downstream velocity profile sampled using a Nortek Vectrino Profiler.

The bed was allowed to run for at least a day until mobile bedforms developed and the size distribution reached statistical stationarity. After this developmental period, each experiment consisted of a 4 day clay free period of sand bed load transport (baseline) followed by one or more clay injections. Baselines were long enough to ensure that enough bedforms were recorded to accurately determine the clay-free average morphodynamic conditions for each run. Relative standard error in measurements of mean bedform height dropped below 5% and 0.4% when 75 and 120 bedforms were measured. We performed four experiments, referred to hereafter as Runs 1-4 (see Table 1 for details). Run 1 consisted of a single clay injection of 1000 g followed by 261.5 hours of bed elevation measurements. Run 2 consisted of an injection of 333 g every four days totaling 277 hours of observations and three injections. Run 3 represented an initial 700 g injection followed by a 300 g clay addition approximately every 1.4 days for the first 300 hours. After 300

hours the observation time between clay injections was increased. Run 4 consisted of a single initial injection of 5500 g followed by 256 hours of observation. The injected clay was kaolinite (Snobrite 75, the Cary Company), with a median listed particle diameter of 0.5 μ m. For Runs 1-3, the clay was mixed with water matching the flume background salinity (350 μ S/cm) in beakers with automatic stirrers for 12 hours prior to the injection. At the background salinity levels, the clay flocculates and the mean D_{50} diameter rises to just above 30 μ m. Due to the large amount of clay added, Run 4 was rapidly mixed over a short period (30 minutes), leading to noticeable amounts of unsuspended clay during the injection. For each injection, the clay was continuously poured into the endwell over the measured recirculation time of the flume (40 s). Following each injection, the system was allowed to evolve and changes in the clay concentration, hyporheic exchange and bedform morphodynamics were observed.

Suspended clay concentration was continuously measured at a one-minute intervals with a Xylem turbidity meter (Runs 1 & 2 - WTW Visoturb 700IQ SW, Runs 3 & 4 - WTW Visolid 700IQ SW) positioned just upstream of the flume endwell (Figure 1a). Concentration measurements for the first 6.75 hrs of Run 1 were taken by hand every hour using a syringe and processed via a spectrophotometer (Hach Company, DR/4000), because initial instream clay concentrations exceeded the measurement range of the Visoturb 700IQ SW. A calibration curve relating known concentrations of kaolinite to the absorbance of 600 nm light was used to determine the concentration of the samples.

The hyporheic exchange flux (HEF) was measured through salt tracer injections during the baseline and following the end of the experiment. To measure HEF freestream salinity was recorded following dissolved NaCl tracer injections, typically 10 hours long, using a salinity meter (SM Star Comm, resolution of 0.01 μ S/cm). The initial HEF was calculated via regression of the rate of decline in salt concentration with time immediately following the NaCl tracer injection, following the methodology of Fox, Boano, and Arnon (2014). No measurement of HEF was performed for the end of Run 4 due to a leak in the flume, which significantly increased the rate of flow into the bed.

Elevation of the sand bed was recorded at a point with an Acoustic Doppler Velocimeter (ADV) profiler and over a large spatial area with two digital single-lens reflex (DSLR) Nikon D5300 cameras. The ADV was positioned in the center of the camera visualization region located 355 cm from the downstream end of the flume (see Figure 1a).

The ADV profiler recorded depth to the sediment bed (2 Hz) from a fixed elevation. Images were taken every minute to visualize bedform propagation and determine bedform length and celerity (see Data Processing, Figure 1b). The cameras were affixed to mounting arms attached to a table adjacent to the flume. They were faced perpendicular to the bed, providing a combined field of view of 180 cm, centered on the profiler and approximately 2.25 times the length of an average bedform. The visualization region was backlit to provide sufficient contrast for automated feature extraction.

At the conclusion of Runs 1-3, 36 cores were taken of the bed following the protocol of Fox et al. (2014) and analyzed for bed clay composition to yield depth averaged clay masses for each 0.5 cm depth interval. In order to extract a core, the flow was stopped, free stream clay was allowed to settle, and the water level was slowly decreased until touching the top of the bed. A syringe was used to remove the settled clay from the surface of the bed by suctioning out the water immediately above the bed in the core measurement region. For two bedforms three cores were taken equally spaced in the cross stream direction at six locations: at the downstream trough, at the crest, and at four equally spaced between the trough and crest. In total 18 cores were taken for each bedform sampled. Each core consisted of a 35 mL syringe, 11 cm long by 2.13 cm wide with the tapered end removed. Each core was carefully inserted into the bed, sealed from the bottom, and removed from the flume. Sediment from the cores were extracted in 0.5 cm increments and mixed with 50 mL of deionized water to create a clay suspension. The mixture was weighed and the concentration was determined via absorbance at 600 nm using a spectrometer (Hach Company, DR/4000). These concentrations were subsequently converted into a clay percentage by mass for each depth slice within the core.

2.2 Data Processing

178

179

180

181

183

184

185

186

187

188

190

192

194

195

196

197

198

199

200

202

203

207

209

The time series of the bed elevation recorded by the ADV profiler was smoothed using a Savitzky-Golay filter (Python 2.7 SciPy, window size of 509 data points, 255 seconds) and processed to remove extraneous noise on the elevation signal. A "find peaks" algorithm (Python 2.7 SciPy) was used to identify both the troughs and the peaks of the bed elevation. The height of individual bedforms (H) was defined as the vertical distance between the bedform peak and downstream (stoss side) trough (Figure 1c). Small transient ripples, persisting for no more than several minutes with H < 0.5 cm were removed from the time series prior to calculating the final bedform statistics. For each run, Ta-

ble 2 shows the number of bedforms identified during both the baseline period and the last four days of data collection.

210

211

212

213

214

215

216

217

218

219

220

221

222

224

226

227

228

229

230

231

232

233

235

236

237

238

239

240

241

242

Bedform length (L) and celerity (C) were obtained by image analysis of the sidewall camera images. Raw images from each camera were thresholded using a simple black white thresholding procedure (MATLAB R2019a) that involved using a manually identified black/white pixel cutoff to determine the sediment water interface. The images from both cameras then were stitched together to extract an elevation profile for the full 180 cm field of view, allowing for the simultaneous visualization of multiple bedforms. Increased freestream clay concentration decreased the light exposure requiring manual calibration of the thresholding algorithm following each clay addition. Stitched images were generated and the black/white pixel cutoff was shifted until the sediment water interface was correctly identified. During data processing, sample images were saved every 100 minutes to ensure that the interface was correctly identified and that clay deposition didn't alter the camera light exposure. The resultant sidewall bed elevation profile was processed to extract bedform height using the same methods developed for the ADV profiler. bedform lengths were calculated as the distance between successive troughs, while celerity was calculated as the slope of a linear regression line fit to a trough's downstream location over time. The bedload sediment flux (Q_t) was determined as Q_t $(t) = \beta \psi c H$ (Bagnold, 1941; Martin & Jerolmack, 2013; McElroy & Mohrig, 2009; Simons, 1965) where the bedforms were approximated as triangles with a shape factor $\beta = 0.5$ (Martin & Jerolmack, 2013). The relative proportion of clay within the bed sediment remained low in all experiments, so the porosity was assumed to remain constant for the sand mass flux calculations ($\psi = 0.48$). Average quantities for the baseline and final set of bedforms are provided in Table 2.

Statistical tests were applied separately to the bedform time series data and between the beginning and end of each run to assess potential differences between the pre and post clay bedform data. First, the degree to which the morphodynamic properties H, L, C, and Q_t changed over time was determined via linear regression. Significance of trends in the baseline and post clay injection time series were assessed by considering the regression p-value where a value greater than $\alpha = 0.05$ was taken to indicate that the trend was not significantly different from zero over time (see Table 3). Second, a Mann-Whitney U test was used to compare whether H, L, C, and Q_t from the final period (final 96 hours) of data collection post clay injection were less than the same metrics collected during the clay free baseline period (initial 96 hours, Table 3). Differences were considered significant for an $\alpha \leq 0.05$. Cumulative distribution functions (CDFs) and kernal density estimation (KDE) were used to visualize distributions and potential changes. The CDFs were used to assess how the addition of clay impacted the entire population of measured and derived bedform quantities. KDE was used to create probability density functions (PDFs) of the trough and bed elevation to assess how these quantities impacted clay accumulation. Gaussian kernels were used with Scott's Rule employed to calculate the estimator bandwidth.

3 Results

The results of the four experiments consist of time series of bed elevation, freestream concentration of clay, and the conductivity of the water column following salt tracer injections. From these data sources we derive bedform morphodynamic variables, clay accumulation within the bed, and the hyporheic exchange flux. The four experimental runs were designed to explore the impact of clay accumulation on a population of mobile bedforms and in turn how these combined effects impacted hyporheic exchange. A secondary aim of these experiments was to determine if the current state of bed morphodynamics depended on the history of clay additions (sequence) or only on the current free stream concentration at any given time. We first discuss the results of the clay deposition rates and within bed patterns of accumulation, and how this impacted hyporheic exchange. Second, we discuss the impact of clay deposition on bedform morphodynamics.

3.1 Hyporheic Exchange and Clay Deposition

The four experimental runs are best conceptualized as two sets of paired experiments based on their total added clay mass (Figure 2a). Runs 1 and 2 consisted of 1000 g of clay, while Runs 3 and 4 consisted of 5500 g of clay. Runs 1 and 4 were single injections, while the 1000 g in Run 2 and 3 consisted of multiple injections. Final mean freestream concentrations over the last five hours of measurement are 66.0%, 76.5%, 88.4%, and 81.5% of the initial concentration for Runs 1-4, respectively (Figure 2a). The multi-injection runs (2 & 3) final freestream concentration exceeds that of their paired single injection run, indicating less deposition overall for the multi-injection runs (Figure 2ab). The absence of storage or loss within the recirculating flume means that persistent decreases in freestream clay concentration can be taken as deposition within the bed (Fig-

275

276

277

278

279

280

281

282

283

284

286

287

288

289

290

291

292

293

295

297

299

300

301

302

306

ure 2b). Comparisons between experiments with the same amount of total mass injected show that runs with multiple injections produce less deposition over time by a factor of 1.3 to 1.55 relative to runs with a single injection. For Runs 1-3, the rate of deposition is initially rapid (111.0 g/hr, 33.8 g/hr and 104.2 g/hr over the first two hours) and is roughly proportional to the injection size. Though the rate of clay accumulation within the bed decreases over time, we did not observe the emergence of a steady state concentration within any of the runs indicating that deposition was ongoing (Figure 2b). Run 4 shows unexpected clay depositional behavior compared to other experiments resulting in an initial increase in deposition on the surface of the bedforms followed decline and eventual stabilization (Figure 2b). The variations in Run 4 may be due to incomplete mixing of the clay prior to the injection as described in the Experimental Methods section. For all Runs short timescale (1-2 hr) periodicity within the freestream clay concentration timeseries (Figure 2a) is a mixture of short-term bedform deposition and remobilization, and sensitivity of the turbidity meter to the changing distance to the bed surface due to the passage of bedforms. Tests in clear water conditions indicate a 15% increase in turbidity over bedform crests compared to troughs.

The impact of clay deposition on the HEF was assessed through the injection of a conservative salt tracer (Figure 3). HEF was computed as the rate of change in freestream tracer concentration immediately after the injection (see Figure 3b inset). Initial tracer injections under baseline (i.e. clay free) conditions show similar early time exchange rates of between 12.1 and 13.5 cm/day (Figure 3 b). Following all clay injections, the HEF declined to between 4.6 and 5.7 cm/day, a decline of between 38% and 42% for all experiments. The long-term salt concentration in the freestream decreases slightly with clay in the bed (Figure 3a), the overall difference in values of normalized conductivity between experiments remains small (less than 1% after 10 hours). Overall, the measured HEF at the conclusion of the experiment is approximately constant regardless of the amount of clay accumulated within the bed (Figure 3b).

Despite a very low Stokes settling velocity ($U_s = 8.10 * 10^{-4}$ m/s) and sufficient shear velocity to keep the clay suspended (Rouse number of 0.08), accumulation within the bed begins almost immediately following injection and accumulates visually in a layer approximately 2 cm below the active region of sand transport (Figure 4). The thickness of the clay accumulation layer is not constant throughout the flume or in a given location over time and depends on the history of bed elevation changes at a specific lo-

cation. Deposition from burial within the troughs and hyporheic flow are functions of local bedform size, while scour from bedforms results in remobilization of previously deposited clay. Because of this, individual sediment cores show variations in overall clay concentration and the variation in concentration depth profile (Figure 4). However when depth profiles are averaged across all cores a clear pattern of accumulation emerges (Figure 5). In aggregate, the concentration of clay increases over the first 3-4 cm within the bed before reaching a peak value that is between 4.2 and 11.6 times the concentration at the top of the mobile layer. The zone of peak concentration persists for between 2-4 cm for all runs, corresponding to the clay layer visible from the flume sidewall (see insets within Figure 1b and 4). The concentration profile then declines rapidly, with very little clay found in the lowest 5 cm of the bed. For Runs 1 and 2, with the same total amount of clay injected, the single injection from Run 1 yielded more clay mass at the most likely scour depth. Runs 1 and 2 show relatively little clay (< 0.2%) accumulation above 0.1 m, while the concentration in Run 3 begins to increase almost immediately with depth. The highest mean clay concentration (0.95% by mass) was observed for Run 3 (Figure 5f) which had a total of 609 g of clay accumulated in the bed by the end of the experiment. Cores were not taken for Run 4 due to a leak in the flume during the run.

As clay deposition and bed scour are both continuous processes, the extent of the accumulation will depend on the time history of bed elevation change (i.e. the mobile layer). The mobile layer can be defined by the probability density function of bed elevation (Figure 4 and 5a-c). The peak in clay concentration coincides with the depth of the most frequent scour rather than the deepest (Figure 5a-f), which indicates that accumulation for these profiles is representative of frequent rather than the rarest events. However, the area of the bed that is always net depositional occurs below the mobile layer (Figure 5). The addition of clay appears to alter the distributions of bed elevation and trough of the mobile layer causing the bed elevation to drop (Figure 5a-c). For all experiments, changes in the PDF of bed elevation are slight, however there is an increase in the frequency of bed elevation just below the most common elevation (0.1 m) of the clay free bed (Figure 5a-c). Larger changes are observed in the PDF of trough elevations, which may be more relevant to clay accumulation due to its relationship with deposition and remobilization. For all runs, there is a slight increase in trough frequency at the most frequent bed elevation with clay. The most drastic change occurs for Runs 1 and

2, where a reduction in the most frequent scour depths (elevation of 0.085 m) was observed (Figure 5a-b). For Run 3, which had 5.5 times more injected clay than Runs 1 and 2, there was a slight reduction in the deepest scour depth though the frequency of the most common scour depth did not change (Figure 5c). A similar response was observed for Run 4 (Figure S4).

3.2 Bedform Morphodynamics

340

341

343

345

346

347

348

349

351

353

355

356

357

358

360

362

370

371

Measurements of bedform morphology were extracted from the ADV profiler (H) and the time lapse images of the flume sidewall (L and C). There are three types of results for the bedform morphology: (1) changes in morphology over time for the baseline and the post clay time series for a given run, (2) statistical distributions of bed morphology for the baseline (96 hrs) and the final 96 hours of each experiment, and (3) average bedform statistics for all runs combined. Throughout the experiments short gaps are present in the profiler records due to a need to power cycle the profiler every four days. Additional gaps in the records occur due to data acquisition computer failures. All gaps in the record represent 105/1783 total hours (6%), and no more than 39.5 hours for any of the individual runs.

Bedforms were populations of low-amplitude dunes with average H, L, and C ranging from 2.28-2.36 cm, 77.67-91.76 cm, and 1.28-1.52 cm/min for the baseline segments (see Table 2). For all runs the baseline bedform H, L, C, and Q_t display a high degree of variability and some periodicity, however (except for C in Run 3) they have no trend with time (see statistical results in Table 3). Following the addition of clay to the flume, average quantities of H, C, and Q_t all decrease over time, while L remains relatively constant (see Figure 6 for results from Run 1 and supplemental Figures S1-S3 for Runs 2-4). By comparing the morphodynamic results after the addition of clay for a given run against their baseline statistics we can account for variation in initial conditions. Clay has a larger impact on C relative to H or L, as C shows the largest proportional decrease (15.9%) for the directly measured variables over time following the introduction of clay (Figure 6c). The largest change occurs for Q_t , a combination of both H and C, which has an average 22.8% decrease relative to the baseline flux following the introduction of clay for all runs (Figure 6d and panel d in Figures S1-S3). The observed decreases, relative to each baseline, in mean H, C and Q_t are statistically significant at an alpha level of 0.05 across all experiments while differences in mean L are not (results of a Mann-

Whitney U tests are shown in Table 3). The smallest changes (largest p-values) in H, C, and Q_t are observed during Run 2, which had the lowest amount of clay accumulation within the bed (239 g) and also experienced the lowest instream concentrations for the majority of the run (three injections at 333 g per injection). The largest changes occurred in Run 4, which had the largest total mass addition (one injection at 5500 g) and the most clay accumulation in the bed (990 g). Due to the variability within the populations of bedforms it can also be useful to consider the entire probability distribution, because the differences in the mean values may not describe the entire behavior of the population of bedforms. The observed decrease (8.9-18.8%) in H occurs primarily through a reduction in the height of bedforms near the median size with minimal change in the height of the smallest or largest bedforms (see Figure 6e for Run 1). However, the observed decrease in C and Q_t are the result of a shift in the entire population of bedforms (Figure 6g-h). An interesting aspect of the observed changes is that the height and celerity change independently of the length, indicating that the bedform's aspect ratio decreases as a result of clay accumulation.

To compare the impact of clay deposition on bedform morphodynamics across runs, we normalize H, L, C, and Q_t by their respective mean value for the pre-clay injection baseline. Normalized bedform height and celerity show consistent declines with total clay accumulation in the bed (Figure S5,S6). The trends are linear, with slopes of -0.00014 $(p < 0.001, R^2 = 0.01)$ and -0.00022 $(p < 0.001, R^2 = 0.094)$, respectively. These slopes indicate that declines in H and C of 0.014% and 0.022% are expected per gram of clay accumulated in the bed. Normalized bedform length shows no change with increasing clay accumulation in the bed (p = 0.67) (Figure S7). As sediment flux is dependent on height and celerity, changes in H and C contribute to a sustained decrease in sediment flux (Figure 7), which decreases with increasing clay accumulation with a trend of -0.00029 (p < 0.001, $R^2 = 0.056$), which results in a 0.029% decline expected per gram of clay. Figure 7 b shows 1-cdf for all four runs for the baseline and the last 100 hours of data. The addition of clay reduced the flux for all scales of bedforms at relatively low percentages of clay accumulation by mass in the bed. Reductions in H, Cand Q_t occur for percentages of clay accumulation by mass in the bed of 0.13, 0.10, 0.24, and 0.40% for Runs 1-4, respectively. These results show that relatively small amounts of cohesive particles impact bedform morphodynamics in nontrivial and quantifiable ways.

4 Discussion

405

407

409

410

411

412

413

414

415

416

418

420

421

422

423

424

425

427

429

430

431

432

433

434

435

436

For clay injected into the free stream there are several modes of interaction with the mobile bed layer. Clay particles can deposit directly within the troughs and in zones of hyporheic flow into the bed (Mooneyham & Strom, 2018; Rehg et al., 2005). Once deposited, clay can settle within the pore spaces and mechanically sort due to bed mobility (Baas et al., 2013). The distribution within the cores suggests a tight coupling between clay deposition and bedform dynamics. Accumulation within the mobile layer occurs through direct deposition and hyporheic flow, while deposition below the mobile layer occurs due to hyporheic exchange and settling within the pore spaces. Accumulation and storage within the mobile layer is necessarily transient. However, the majority of deposition occurs here and the association of the peak clay concentrations with the most frequent (the average) scour depth indicates that scour is both a mechanism of deposition and remobilization. Visually from the sidewall of the flume, the accumulation occurs in an approximately two-centimeter thick white band (Figure 4 inset), while the accumulation above and below this layer is not as distinct. Inherent system variability demonstrates that single point measurements, both in the lab and in the field, are not representative of the actual system dynamics. The coupled nature of the system only emerges when averaging over enough cores to reduce the variability associated with the fluctuations of the bed elevation or recent deep scour (see Figure 4). Bedforms deform and change shape as they propagate (McElroy & Mohrig, 2009) such that a deep scour event in one location may not propagate the length of the flume or river reach. Despite this variability, the shape of the accumulation profiles and their correlation with the average bedform scour is consistent across runs.

Differences in the total clay deposited between experiments (Figure 5) depend on the magnitude and time history of the free stream clay concentration. The magnitude of clay injection alters the dynamics of bedform scour. The 1000 g injections (Runs 1-2) reduce the frequency of the average scour depth while in 5500 g injections (Run 3-4) the bed adjusts through a reduction in the deepest scour depths without any reduction in frequency of the average scour depth(Figure 5a-c). Interestingly, the three-injections of Run 2 accumulated more clay at the depth of average scour than Run 1, while depositing less clay overall. Multiple injections allow hyporheic flow to push clay further into the bed prior to clogging (Note concentration below 0.05 in Figure 5e), while large single injections impact HEF more rapidly and restrict clay penetration (Figure 5d). The

438

439

440

442

443

444

445

446

447

448

449

450

451

452

453

455

456

457

458

460

462

466

467

469

overall difference between single vs multiple injections cannot be fully explored as we were unable to take cores for Run 4 due to a leak in the flume. It is important to note that all morphodynamic data presented in this paper for Run 4 were collected before the leak started. Run 4 may have behaved differently due the observed rapid deposition of clay effectively coating the surface flume effectively after the injection. This differing initial condition does not seem to impact the final morphodynamic results (Figure 7) as the clay deposited on the surface was eventually resuspended. The observed decreases in H, Cand Q_t are proportional to the amount of clay accumulated within the bed (Figure 6, 7), S1-6. That freestream clay affects morphodynamics indicates a pathway for hyporheic flow to alter morphodynamics. Clay accumulation depends on both hyporheic flow and morphodynamics; bed sediment flux is also a function of clay accumulation and thus is modulated by hyporheic exchange in the presence of fine particles. Clay accumulation lead to a reduction in H and C, but not L in our experiments. These adjustments are counter to commonly observed adjustments where reductions in height are typically accompanied by decreases in length and an increase in celerity (Bradley & Venditti, 2017; Martin & Jerolmack, 2013). The lack of a noticeable change in length is peculiar, however similar results have been observed for sand beds that have been premixed with cohesive material (both biotic and clay) (Baas et al., 2013; Malarkey et al., 2015).

The morphodynamic change within these experiments likely results from the overall increase in bed cohesiveness caused by the presence of clay. In clay rich cohesive beds (clay % > 30), bonds between clay particles and water molecules act as bridges between sand grains and increase cohesive strength when exposed to shear (Ikari & Kopf, 2011). This increases the shear velocity required for transporting sediment. Even small fractions of clay can meaningfully increase the cohesion of the bed at low percentages (Lichtman et al., 2015; Mitchener & Torfs, 1996; Panagiotopoulos, Voulgaris, & Collins, 1997). However, a precise threshold for when clay content becomes significant has not been identified, as these dynamics depend on diverse system properties such as grain size (Panagiotopoulos et al., 1997) and biological colonization of the sediments (Malarkey et al., 2015). In our experiments, the creation of a less-mobile, highly-cohesive clay layer just beneath the mobile bedforms limits scour depth and decreases hyporheic exchange, which reduces bedform heights and leads to the persistent presence of clay in the mobile layer. This effect has also been observed in pre-mixed clay/sand beds allowed to develop under a clay-free overlying flow (Baas et al., 2013). At clay contents less than 13% clay by

dry weight, Baas et al. (2013) found no change in length and a decrease in height and sediment flux for the mixed-material bedforms, consistent with our current findings.

470

471

472

473

475

476

477

478

479

480

481

482

484

486

487

488

489

491

493

497

400

500

501

We confirmed that decreases in bedform height, celerity and sediment flux are caused by increased bed cohesion, rather than changes in fluid properties of the suspension. Increasing the kaolinite concentration of a suspension increases the viscosity (Wan, 1985). At large concentrations, this leads to hyperconcentrated non-Newtonian flow that flattens the bed and decreases bedform height (Baas et al., 2011; Wan, 1985). However, at lower concentrations (< 262 g/L), modulation of freestream turbulence by clay particles increases the bedform height (Baas et al., 2011). The freestream concentration in our experiments barely exceeds 10 g/L at the largest. Moreover, an increase in viscosity without changing the Newtonian behavior of a fluid causes bedform celerities and heights to increase (Southard, 1991). We observe that changes in morphodynamic properties are correlated with clay in the bed, not with clay in the freestream (Figure 7, S5 and S6). Taken together, this evidence indicates that increased bed cohesion is the dominant process that modifies bedform dynamics, and this process counteracts changes in flow turbulence and viscosity that would otherwise increase bedform heights and celerities.

The impact of clay on the cohesion of bedforms appears to be independent of the method of mixing or interaction as the strong decrease in flux for moderate decreases in other morphodynamic properties is also observed for initially pre-mixed clay sand mixtures (Baas et al., 2013) at higher clay fractions within the bed. The current findings show a larger impact on morphodynamics for a given clay mass and indicate that longer experiments are necessary to capture these slower interactions. A linear extrapolation shows that a height decrease of 14% is expected for 1000g in the bed (0.04% of the total bed by dry weight) while a similar drop could be expected by Baas et al. (2013) if the slurry mixture was 5.77% clay by dry weight. This large discrepancy (0.04% vs 5.77% clay) can be partially accounted for by considering only the clay in the accumulation layer and mobile layer where concentrations are higher. However, even in the center of the clay accumulation layer, the clay fraction never exceeds 2%. The short duration of the Baas et al. (2013) experiments (< 3 hr) compared to the current experiments (> 350 hr) are likely responsible for the differences, as large numbers of bedforms are needed to characterize observed changes. Further, similar bedform adjustment occurs in both sets of experiments, indicating that the observed changes in morphodynamics may not depend

strongly on either the pathway through which clay enters the bed or the system initial conditions.

Our findings challenge previous conceptions of fine particles as simply washload. Fully suspended clay particles both deposit in sand beds and alter the bed morphodynamics. For a constant stream flow rate, the injection of fine particles leads to permanent storage of clay in a layer immediately below the region of mobile sand transport, resulting in persistent changes in system morphodynamics. The formation and temporal variation of this layer has implications for the accumulation of fine particles in openframework sediment beds, an area of emerging concern for riverine ecosystems (Wharton, Mohajeri, & Righetti, 2017) as the strong depth variation in fine particles has ramifications for biotic communities impacted by siltation. For systems with active sand transport, the depth of the clay layer is related to the scour dynamics of the preceding bedforms. In beds with active sand transport, multiple sediment cores at different temporal and spatial locations need to be taken to ensure that accurate conclusions are drawn concerning particle deposition profiles.

Unlike in the current flume experiments, natural bedforms are rarely in equilibrium with the flow (Myrow, Jerolmack, & Perron, 2018). This is especially true during flood events when discharge is extremely variable. Even if the bedforms are not in perfect equilibrium, the accumulation of fines in the bedforms is expected to reduce the bedload sediment transport rates. Further, the results presented here demonstrate that clay deposits are highly focused in a layer beneath bedforms, and that localized clay accumulation in this region is much more important than overall mass fraction of clay in the bed. Future work should investigate the interactions of natural discharge variations with clay inputs into rivers, patterns of clay accumulation, and bedform morphodynamics.

In conclusion, significant deposition and alteration of bed morphodynamics indicates a previously unrecognized role of initially suspended fine particles and hyporheic flow on bed morphodynamics. These experiments demonstrate that fine cohesive particles, even in relatively low concentrations, reduce the bedform sediment flux. Clay accumulation in the bed occurs both through hyporheic flow and burial within the bedform troughs, which collectively decrease the height, celerity, and sediment flux of the mobile bedforms. Clay accumulation alters the celerity and shape of the bedforms independently as larger decreases in celerity result in only slight decreases in height, and

no observed changes in length. Typically, decreases in bedform height and length occur 534 together and result in increased celerity (Martin & Jerolmack, 2013). These observations 535 indicate the existence of a complex set of coupled dynamics and feedbacks between hyporheic exchange, sand bed mobility, and suspended fine particle dynamics. Understand-537 ing the sediment dynamics in rivers requires models capable of coupling bed morphodynamics, hyporheic flow, and fine particle deposition. Such modeling will build a more 539 accurate picture of the ecological and geological impacts of fine particle deposition, which 540 is needed as anthropogenic activity is increasing fine particle concentration in rivers world-541 wide. 542

Acknowledgments

543

549

We thank M. Payne for laboratory assistance. We thank J. Baas, T. Swanson, and an
anonymous reviewer for constructive reviews that improved this manuscript. Research
was supported by the NSF-BSF Joint Program in Earth Sciences (EAR-1734300). Data
are publicly available from the Hydroshare repository (https://www.hydroshare.org/resource/
73c79ca44f3340c39a550e8f6ddb1bf7).

References

- Ansari, A. (2005). Eutrophication: causes, consequences and control. Dordrecht;

 New York: Springer.
- Baas, J. H., & Best, J. L. (2002). Turbulence modulation in clay-rich sediment-laden flows and some implications for sediment deposition. *Journal of Sedimentary Research*, 72(3), 336–340.
- Baas, J. H., & Best, J. L. (2008). The dynamics of turbulent, transitional and laminar clayladen flow over a fixed current ripple. Sedimentology, 55(3), 635–666.
- Baas, J. H., Best, J. L., & Peakall, J. (2011). Depositional processes, bedform development and hybrid bed formation in rapidly decelerated cohesive (mudsand) sediment flows. *Sedimentology*, 58(7), 1953–1987.
- Baas, J. H., Davies, A. G., & Malarkey, J. (2013). Bedform development in mixed sandmud: The contrasting role of cohesive forces in flow and bed. *Geomorphology*, 182.
- Bagnold, R. A. (1941). The physics of blown sand and desert dunes. London:

 Methuen Publishing.

```
Belmont, P., Gran, K. B., Schottler, S. P., Wilcock, P. R., Day, S. S., Jennings, C.,
565
            ... Parker, G. (2011). Large shift in source of fine sediment in the upper mis-
566
                            Environmental Science & Technology, 45(20), 8804–8810. doi:
            sissippi river.
            10.1021/es2019109
568
      Best, J. (2005).
                           The fluid dynamics of river dunes: A review and some future re-
            search directions. Journal of Geophysical Research: Earth Surface, 110. doi:
570
            10.1029/2004JF000218
571
       Bilotta, G. S., & Brazier, R. E. (2008). Understanding the influence of suspended
572
            solids on water quality and aquatic biota. Water Research, 42(12), 2849-2861.
573
            doi: 10.1016/j.watres.2008.03.018
574
       Boano, F., Harvey, J. W., Marion, A., Packman, A. I., Revelli, R., Ridolfi, L., &
575
                                      Hyporheic flow and transport processes: Mechanisms,
            Wörman, A.
                            (2014).
            models, and biogeochemical implications.
                                                         Review of Geophysics, 52, 603-679.
577
            doi: 10.1002/2012RG000417
578
      Bradley, R. W., & Venditti, J. G.
                                             (2017).
                                                        Reevaluating dune scaling relations.
579
            Earth-Science Reviews, 165, 356–376. doi: 10.1016/j.earscirev.2016.11.004
580
       Chapman, D. W. (1988). Critical review of variables used to define effects of fines
581
            in redds of large salmonids.
                                            Transactions of the American Fisheries Society,
582
            117(1), 1-21. doi: 10.1577/1548-8659(1988)117\langle 0001:CROVUT \rangle 2.3.CO; 2
583
       Drummond, J. D., Aubeneau, A. F., & Packman, A. I. (2014).
                                                                          Stochastic model-
584
            ing of fine particulate organic carbon dynamics in rivers. Water Resources Re-
585
            search, 50(5), 4341-4356.
586
       Drummond, J. D., Larsen, L. G., Gonzalez-Pinzon, R., Packman, A. I., & Harvey,
            J. W. (2018). Less fine particle retention in a restored versus unrestored urban
588
            stream: Balance between hyporheic exchange, resuspension, and immobiliza-
            tion. Journal of Geophysical Research: Biogeosciences, 123(4), 1425-1439. doi:
590
            10.1029/2017JG004212
591
       Elliot, A., & Brooks, N. (1997). Transfer of nonsorbing solutes to a streambed with
592
            bed forms: Theory. Water Resources Research, 33(1), 123–136.
593
       Feris, K., Ramsey, P., Frazar, C., Moore, J. N., Gannon, J. E., & Holben, W. E.
            (2003).
                       Differences in hyporheic-zone microbial community structure along a
595
            heavy-metal contamination gradient. Applied and Environmental Microbiology,
```

69(9).

```
Feris, K., Ramsey, P. W., Rillig, M., Moore, J. N., Gannon, J. E., & Holben, W. E.
598
                       Determining rates of change and evaluating group-level resiliency dif-
599
            ferences in hyporheic microbial communities in response to fluvial heavy-metal
            deposition. Applied and Environmental Microbiology, 70(8).
601
       Foster, I. D. L., & Charlesworth, S. M. (1996). Heavy metals in the hydrological cy-
             cle: Trends and explanation. Hydrological Processes, 10(2), 227-261. doi: 10
603
             .1002/(\text{SICI})1099-1085(199602)10:2\langle 227::\text{AID-HYP357}\rangle 3.0.\text{CO}; 2-\text{X}
604
       Fox, A., Boano, F., & Arnon, S.
                                          (2014).
                                                     Impact of losing and gaining streamflow
605
            conditions on hyporheic exchange fluxes induced by dune-shaped bed forms.
606
             Water Resources Research, 50(3), 1895-1907. doi: 10.1002/2013WR014668
607
       Fox, A., Packman, A. I., Boano, F., Phillips, C. B., & Arnon, S.
608
            actions between suspended kaolinite deposition and hyporheic exchange flux
            under losing and gaining flow conditions. Geophysical Research Letters, 45(9),
610
            4077-4085. doi: 10.1029/2018GL077951
611
       Greig, S. M., Sear, D. A., & Carling, P. A.
                                                      (2005).
                                                                 The impact of fine sediment
612
            accumulation on the survival of incubating salmon progeny: Implications for
613
                                         Science of the Total Environment, 344(1), 241-258.
            sediment management.
614
             doi: 10.1016/j.scitotenv.2005.02.010
615
       Hartwig, M., & Borchardt, D. (2015). Alteration of key hyporheic functions through
616
            biological and physical clogging along a nutrient and finesediment gradient.
617
             Ecohydrology, 8(5), 961-975. doi: 10.1002/eco.1571
618
       Harvey, J. W., Drummond, J. D., Martin, R. L., McPhillips, L. E., Packman, A. I.,
619
            Jerolmack, D. J., ... Tobias, C. R.
                                                   (2012).
                                                            Hydrogeomorphology of the hy-
            porheic zone: Stream solute and fine particle interactions with a dynamic
621
                           Journal of Geophysical Research: Biogeosciences, 117(G4).
            streambed.
                                                                                          doi:
             10.1029/2012JG002043
623
       Horowitz, A.
                        (2009).
                                   Monitoring suspended sediments and associated chemical
624
            constituents in urban environments: lessons from the city of atlanta, georgia,
625
             usa water quality monitoring program.
                                                       Journal of Soils and Sediments, 9(4),
626
            342 - 363.
627
```

Karwan, D. L., Aalto, R., Aufdenkampe, A. K., Denis Newbold, J., & Pizzuto, J. E.

cal Research Letters, 38(16).

Ikari, M. J., & Kopf, A. J. (2011). Cohesive strength of clayrich sediment. Geophysi-

628

629

(2011). Characterization and source determination of stream suspended partic-631 ulate material in white clay creek, USA. Applied Geochemistry, 26, S354–S356. 632 doi: 10.1016/j.apgeochem.2011.03.058 Karwan, D. L., & Saiers, J. E. (2012).Hyporheic exchange and streambed filtra-634 tion of suspended particles. Water Resources Research, 48(1). doi: 10.1029/ 2011WR011173 636 Li, A., Aubeneau, A. F., Bolster, D., Tank, J. L., & Packman, A. I. (2017).Co-637 variation in patterns of turbulencedriven hyporheic flow and denitrification 638 enhances reachscale nitrogen removal. Water Resources Research, 53(8), 639 6927 - 6944.640 Lichtman, I. D., Baas, J. H., Amoudry, L. O., Thorne, P. D., Malarkey, J., Hope, 641 J. A., ... Ye, L. (2015). Bedform migration in a mixed sand and cohesive clay intertidal environment and implications for bed material transport predictions. 643 Geomorphology, 315, 17-32. doi: 10.1002/eco.1571 644 Lloyd, D. S., Koenings, J. P., & Laperriere, J. D. (1987). Effects of turbidity in fresh 645 waters of alaska. North American Journal of Fisheries Management, 7(1), 18-646 33. 647 Louhi, P., Ovaska, M., Maki Petays, A., Erkinaro, J., & Muotka, T. (2011).Does 648 fine sediment constrain salmonid alevin development and survival? Canadian649 Journal of Fisheries and Aquatic Sciences, 68(10), 1819-1826. doi: 10.1139/ 650 f2011-106 651 Malarkey, J., Baas, J. H., Hope, J. A., Aspden, R. J., Parsons, D. R., Peakall, J., . . . 652 Thorne, P. D. (2015).The pervasive role of biological cohesion in bedform development. Nature Communications, 6, 6257. doi: 10.1038/ncomms7257 654 Martin, R. L., & Jerolmack, D. J. (2013). Origin of hysteresis in bed form response 655 to unsteady flows. Water Resources Research, 49(3), 1314-1333. doi: 10.1002/ 656 wrcr.20093 657 McElroy, B., & Mohrig, D. (2009).Nature of deformation of sandy bed 658 forms. Journal of Geophysical Research: Earth Surface, 114(F3). doi: 659 10.1029/2008JF001220 Merill, L., & Tonjes, D. J. (2014). A review of the hyporheic zone, stream restora-661 tion, and means to enhance denitrification. Critical Reviews in Environmental 662

Science and Technology, 44(21).

- Mitchener, H., & Torfs, H. (1996). Erosion of mud/sand mixtures. Coastal Engineering, 29, 1-25.
- Mooneyham, C., & Strom, K. (2018). Deposition of Suspended Clay to Open and
 Sand-Filled Framework Gravel Beds in a Laboratory Flume. Water Resources

 Research, 54(1), 323–344. doi: 10.1002/2017WR020748
- Mueller, E. R., & Pitlick, J. (2013). Sediment supply and channel morphology in mountain river systems: 1. relative importance of lithology, topography and climate. *Journal of Geophysical Research: Earth Surface*. doi: 10.1002/2013JF002843
- Myrow, P. M., Jerolmack, D. J., & Perron, J. T. (2018). Bedform disequilibrium.

 Joural of Sedimentary Research, 88(9), 1096-113.
- Nelson, E. J., & Booth, D. B. (2002). Sediment sources in an urbanizing, mixed land-use watershed. *Journal of Hydrology*, 264, 51–68.
- Owens, P. N., Batalla, R. J., Collins, A. J., Gomez, B., Hicks, D. M., Horowitz,

 A. J., ... Trustrum, N. A. (2005). Fine-grained sediment in river systems:

 environmental significance and management issues. River Research and Appli-

cations, 21(7), 693-717. doi: 10.1002/rra.878

680

- Packman, A. I., Brooks, N., & Morgan, J. (2000b). A physicochemical model for colloid exchange between a stream and a sand streambed with bed forms. Water

 Resources Research, 36(8), 2351–2361.
- Packman, A. I., Brooks, N., & Morgan, J. (2001). Hyporheic exchange of solutes and colloids with moving bed forms. Water Resources Research, 37(10), 2591– 2605.
- Packman, A. I., Brooks, N. H., & Morgan, J. J. (2000a). Kaolinite exchange between a stream and streambed; laboratory experiments and validation of a colloid transport model. Water Resources Research, 36(8), 2363–2372.
- Packman, A. I., & Mackay, J. S. (2003). Interplay of streamsubsurface exchange, clay particle deposition, and streambed evolution., 39(4).
- Paerl, H. W., & Otten, T. G. (2013). Harmful cyanobacterial blooms: causes, consequences, and controls. *Microbial Ecology*, 65(4).
- Panagiotopoulos, I., Voulgaris, G., & Collins, M. (1997). The influence of clay on the threshold of movement of fine sandy beds. *Coastal Engineering*, 32, 19-43.
 - Phillips, C. B., Dallmann, J. D., Jerolmack, D. J., & Packman, A. I. (2019).

- Fineparticle deposition, retention, and resuspension within a sandbedded stream are determined by streambed morphodynamics. Water Resources

 Research, 10, 303-318.
- Rehg, K. J., Packman, A. I., & Ren, J. (2005). Effects of suspended sediment characteristics and bed sediment transport on streambed clogging. *Hydrological Processes*, 19(2), 413–427.
- Rose, L. A., Karwan, D. L., & Godsey, S. E. (2018). Concentration discharge relationships describe solute and sediment mobilization, reaction, and transport at event and longer timescales. *Hydrological Processes*, 32(18), 2829–2844. doi: 10.1002/hyp.13235
- Ryan, P. A. (1991). Environmental effects of sediment on new zealand streams: A review. New Zealand Journal of Marine and Freshwater Research, 25(2), 207–221.
- Sekely, A. C., Mulla, D. J., & Bauer, D. W. (2002). Streambank slumping and its contribution to the phosphorus and suspended sediment loads of the blue earth river, minnesota. *Journal of Soil and Water Conservation*, 57(5), 243-250.
- Simons, D. B. (1965). Bedload equation for ripples and dunes [Book]. Washington:

 Washington: United States Department of the Interior, Geological Survey.
- Smith, J. D., & McLean, S. R. (1977). Spatially averaged flow over a wavy surface. Journal of Geophysical Research, 82(12), 1735-1746. doi: 10.1029/ JC082i012p01735
- Southard, J. (1991). Experimental determination of bed-form stability. Annual Review of Earth and Planetary Science, 55(8), 423-455.
- Thibodeaux, L. J., & Boyle, J. D. (1987). Bedform-generated convective transport in bottom sediment. *Nature*, 325 (6102).
- Vaughan, A. A., Belmont, P., Hawkins, C. P., & Wilcock, P. (2017). Near-channel versus watershed controls on sediment rating curves. *Journal of Geophysical Research: Earth Surface*, 122(10), 1901–1923. doi: 10.1002/2016JF004180
- Wan, Z. (1984). The bed material movement in hyperconcentrated flow. *Journal of Hydraulic Engineering* (8), 1-14.
- Wan, Z. (1985). Bed material movement in hyperconcentrated flow. *Journal of Hy-*draulogical Engineering, 111(6), 987-1002.

Wharton, G., Mohajeri, S. H., & Righetti, M. (2017). The pernicious problem

of streambed colmation: a multi-disciplinary reflection on the mechanisms, 730 causes, impacts, and management challenges. Wiley Interdisciplinary Reviews: 731 Water, 4(5), e1231. doi: 10.1002/wat2.1231 732 Wolman, M. G. (1967).A Cycle of Sedimentation and Erosion in Urban River 733 Channels. Geografiska Annaler. Series A, Physical Geography, 49(2/4), 385-734 395. 735 Wood, P. J., & Armitage, P. D. (1997).Biological effects of fine sediment in the 736 lotic environment (Vol. 21). Berlin/Heidelberg. doi: 10.1007/s002679900019 737 Zhang, H., Feng, X., Larssen, T., Shang, L., Vogt, R. D., Lin, Y., ... Zhang, H. 738 (2010).Fractionation, distribution and transport of mercury in rivers and 739 tributaries around wanshan hg mining district, guizhou province, southwestern 740 china: Part 2 methylmercury. Applied Geochemistry, 25(5), 642–649.



Run 1	Run 2	Run 3	Run 4
99.5	98	100	100
261.5	277	586	256
1	3	17	1
1000	333	300^{a}	5500
1000	1000	5500	5500
	99.5 261.5 1 1000	99.5 98 261.5 277 1 3 1000 333	99.5 98 100 261.5 277 586 1 3 17 1000 333 300 ^a

Table 1. Information concerning the experimental setup for all 4 runs. Each run consists of a baseline without clay after which the first clay injection was conducted. The post baseline period occurs after this first injection. The number of injections (including the initial injection) and the size of each injection are shown.

^a This run consisted of two closely timed initial injections of 700 and 300 g followed by regular injections of 300g



Run	t	C_B	Н	L	C	Q_t	N	HEF
Base-1	362	0	0.0227	0.777	0.770	0.00541	146	12.1
Base-2	379	0	0.0235	0.918	0.904	0.00624	175	12.5
Base-3	686^a	0	0.0234	0.865	0.870	0.00603	169	13.5
Base-4	356	0	0.0223	0.838	1.039	0.00681	156	${\rm N}/{\rm A}^b$
Clay - 1	362	322	0.0205	0.730	0.634	0.00400	146	4.6
Clay-2	379	239	0.0214	0.825	0.835	0.00556	128	4.7
Clay-3	686^a	609	0.0209	0.796	0.763	0.00486	132	5.7
Clay-4	356	990	0.0181	0.805	0.769	0.00442	143	${\rm N}/{\rm A}^b$

Table 2. Experiment and bedform statistics for all 4 runs. The total length of the entire run (baseline and post baseline) is given by t and measured in hours. The first 4 rows represent clay-free baseline data and the last 4 represent data taken after clay injection. Each measurement period is 4 days long. For the baseline data, the clay mass in the bed - C_B (g) is 0, while for the clay runs C_B represents the average clay in the bed over the final 4 day window. H, L, C, and Q_t are averages of bedform height (m), length (m), celerity (m/hr), and sediment flux (m^2/hr) for the initial 96 hours (Base) and final 96 hours (Clay). N is the number of bedforms measured during each 4 day period as recorded by the ADV profiler. HEF is the hyporheic exchange flux cm/day.

^aTime here is the duration of the entire run. Because of a camera data collection failure near the end of the run (see Figure S2), results in this table were gathered for the contiguous 4-day period preceding the failure (479-575 hours)

^bDue to a flume leak, it was impossible to obtain final hyporheic exchange data for this run.

Run	$P_H (R_H^2)$	$P_L (R_L^2)$	$P_c (R_c^2)$	$P_q \ (R_q^2)$
Base-1	0.96 (0.00)	0.75 (0.00)	0.78 (0.00)	0.22 (0.01)
Base-2	0.56 (0.00)	0.40 (0.00)	$0.16 \ (0.02)$	0.90 (0.00)
Base-3	0.90 (0.00)	0.31 (0.01)	< 0.01 (0.15)	$0.03 \ (0.04)$
Base-4	0.70 (0.00)	0.38 (0.00)	$0.25 \ (0.01)$	0.51 (0.00)
Clay - 1	0.74 (0.00)	0.09 (0.01)	< 0.01 (0.08)	0.01 (0.02)
Clay-2	0.72 (0.00)	0.59 (0.00)	0.81 (0.00)	$0.72\ (0.00)$
Clay - 3	0.01 (0.01)	0.40 (0.00)	$0.02\ (0.01)$	< 0.01 (0.03)
Clay-4	0.14 (0.01)	0.82 (0.00)	< 0.01 (0.04)	< 0.01 (0.03)
Mean-1	0.016	0.390	< 0.001	< 0.001
Mean-2	0.045	0.131	< 0.001	0.005
Mean-3	0.011	0.436	< 0.001	0.005
Mean-4	0.010	0.330	< 0.001	< 0.001

Table 3. The rows labeled Base and Clay contain the statistical results of linear regressions (P-values and R^2 values) for trends over time within the baseline and post-clay injection bedform morphologies $(H, L, C, \text{ and } Q_t)$. Rows labeled Mean- represent results (P-values) of Mann-Whitney U tests between the mean of the baseline and final 96 hours of bedforms in the presence of clay for H, L, C, and Q_t .

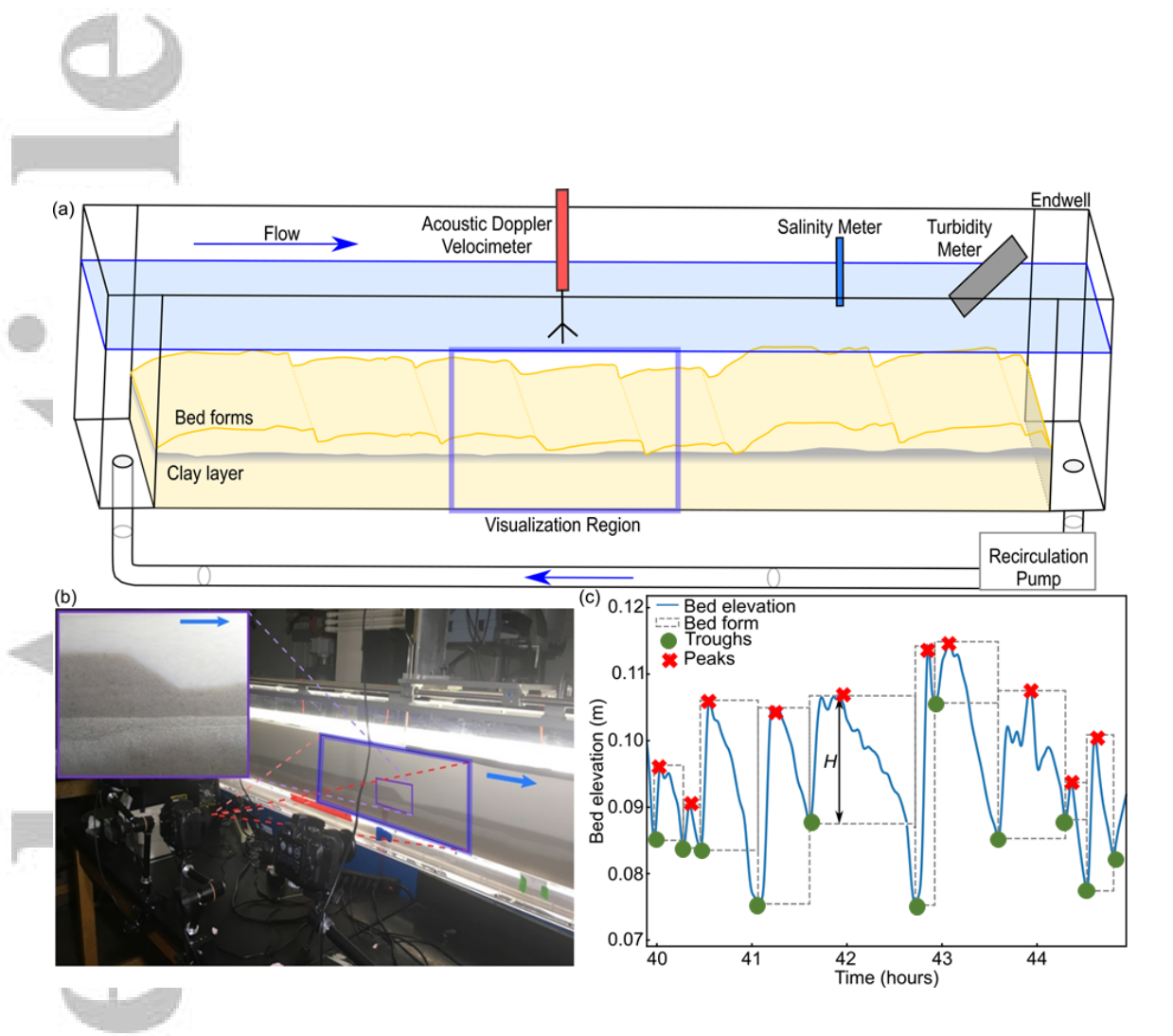


Figure 1. Schematic diagrams of experimental setup and data processing. (a) Schematic of the experimental setup (flow is from left to right). The foreground bedform profile and location of the clay layer represent a partial trace from sidewall images during an experiment. Experimental measurement devices are located in their approximate locations. A porous endplate maintains a minimum sand bed elevation while allowing hyporheic flow to pass. The blue rectangle represents the visualization region of the sidewall camera setup shown in (b). (b) Sidewall imaging set up bedforms following clay injection during Run 3. The blue rectangle represents the FOV of the cameras. The ADV profiler is positioned on a cart directly above the center of the camera FOV. The inset (purple border) shows a close up of a bedform crest and trough and the accumulation of clay below the mobile layer. (c) Smoothed bedform elevation data from the ADV profiler showing the extracted bedform heights (peak to trough) identified for a portion of Run 1. Note that small bedform ripples (see structure at 44.4 hrs) are not treated as individual bedforms.

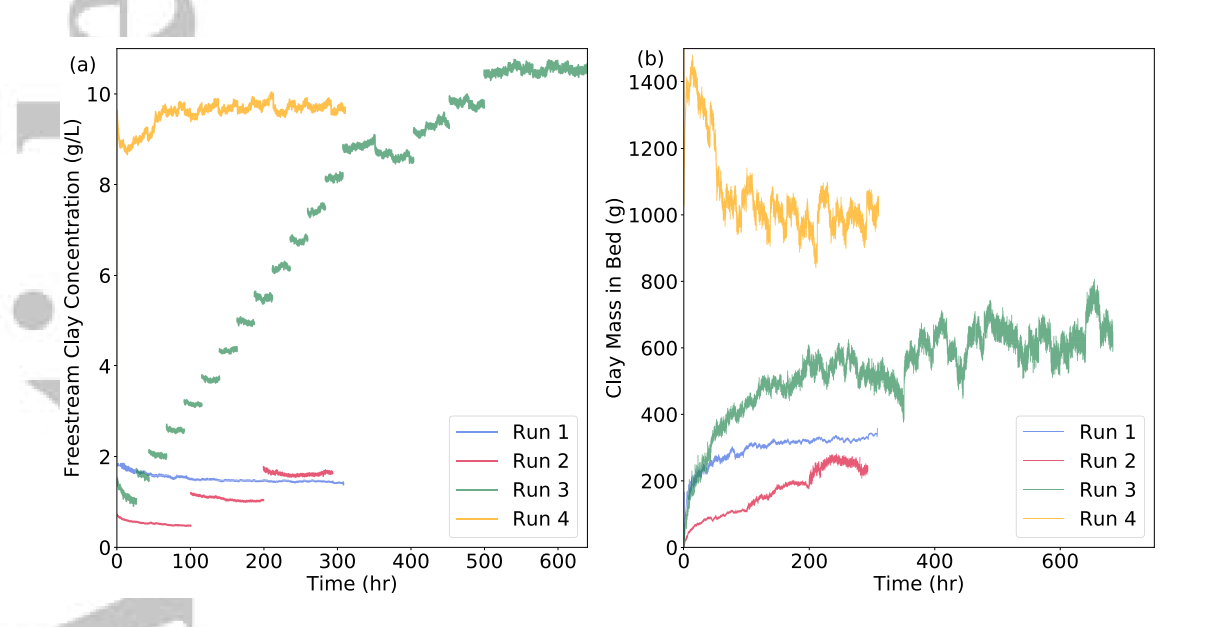


Figure 2. Patterns of clay deposition. (a) Timeseries of freestream clay concentrations for Runs 1-4. Jumps in freestream concentration reflect clay injections. (b) Accumulation of clay within the bed over time.

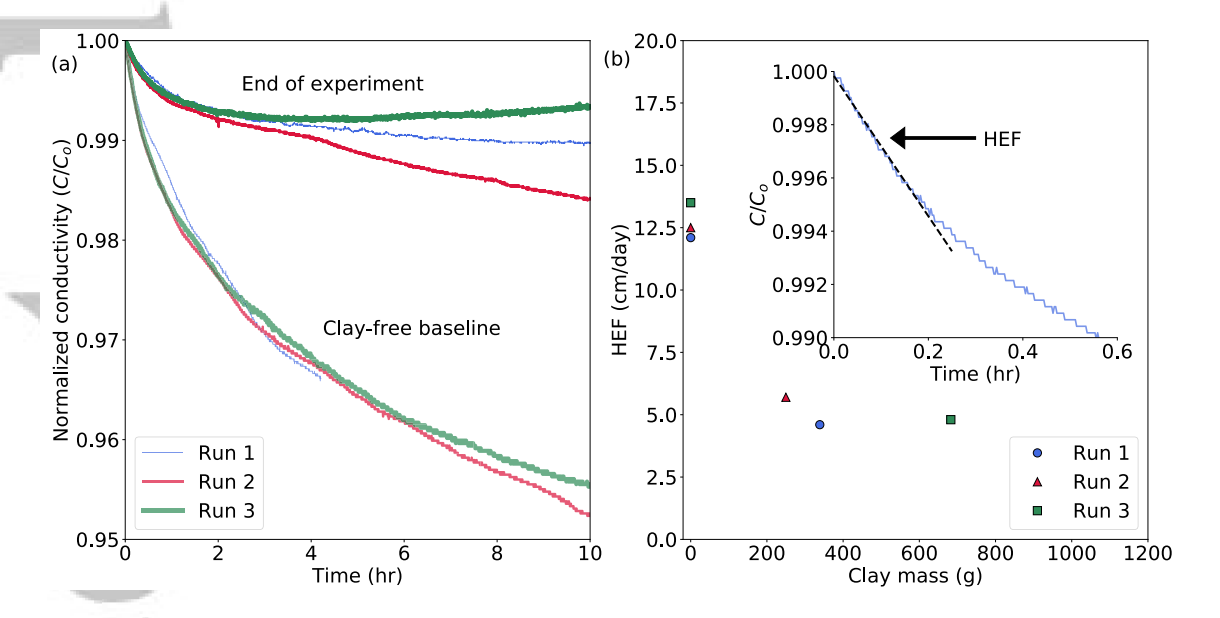


Figure 3. Decreasing hyporheic exchange with increasing clay deposition. A hyporheic exchange measurement was not made for Run 4 due to a flume leak just before the exchange measurement that pulled excessive clay into the subsurface. (a) Normalized freestream salt concentration following the clay-free baseline (lower 3 curves) and end of experiment (upper 3 curves). (b) Hyporheic exchange flux as a function of clay mass deposited in the bed. The inset shows how the HEF is calculated as the slope of the normalized concentration following the injection.

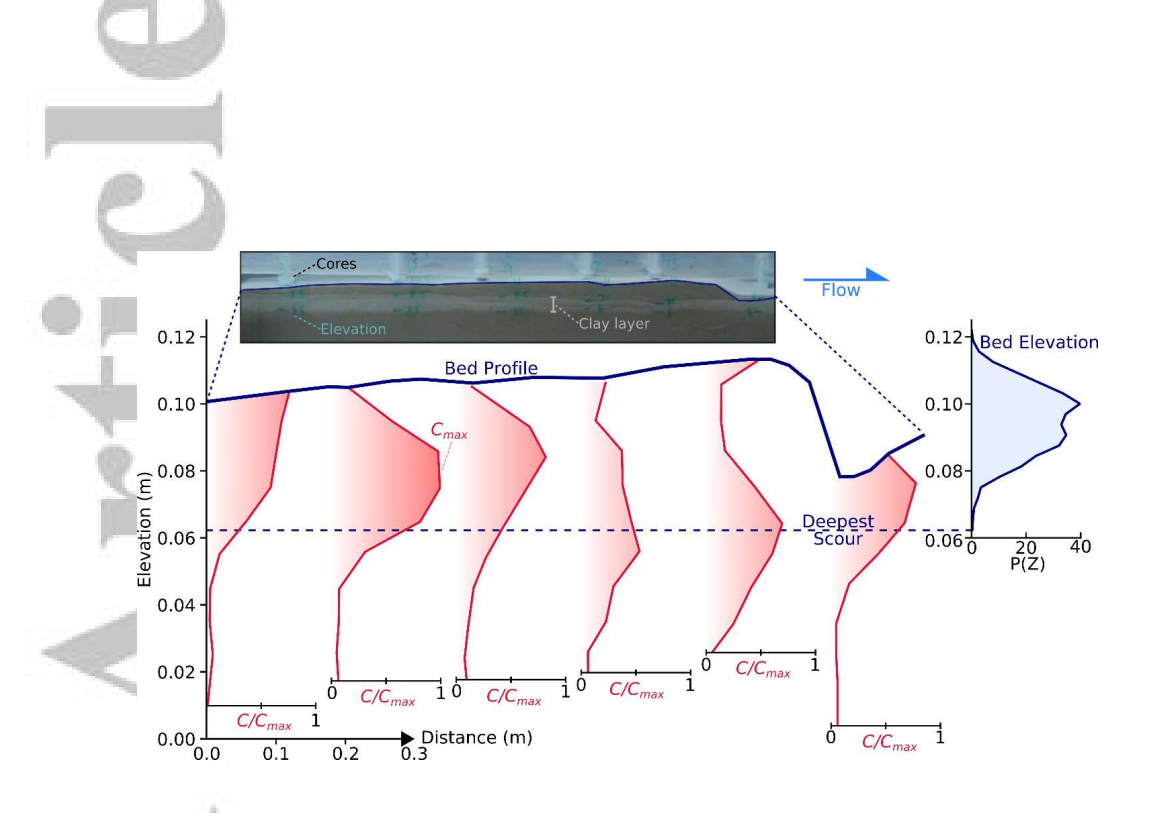


Figure 4. Visualization of clay accumulation for a single experimental bedform from Run 1. The bold blue line represents the surface of an experimental bedform at the end of a run traced from the sidewall (see inset for photograph of the bedform). The bed profile is not to scale as the downstream distance has been compressed by a factor of approximately nine relative to the vertical dimension. The PDF of elevation to the right of the profile represents the complete probability of surface elevation location for the entirety of the run following the clay injections. The deepest scour is the lowest recorded elevation and is denoted by the blue dashed line. The red vertical lines and shading represent the average clay concentration of three cores in the cross-stream direction normalized by the maximum observed concentration for the whole bedform. The zero-concentration point represents the approximate location of the core on the bed profile. The inset above the figure shows this bedform from a sidewall view. Flow is from left to right.

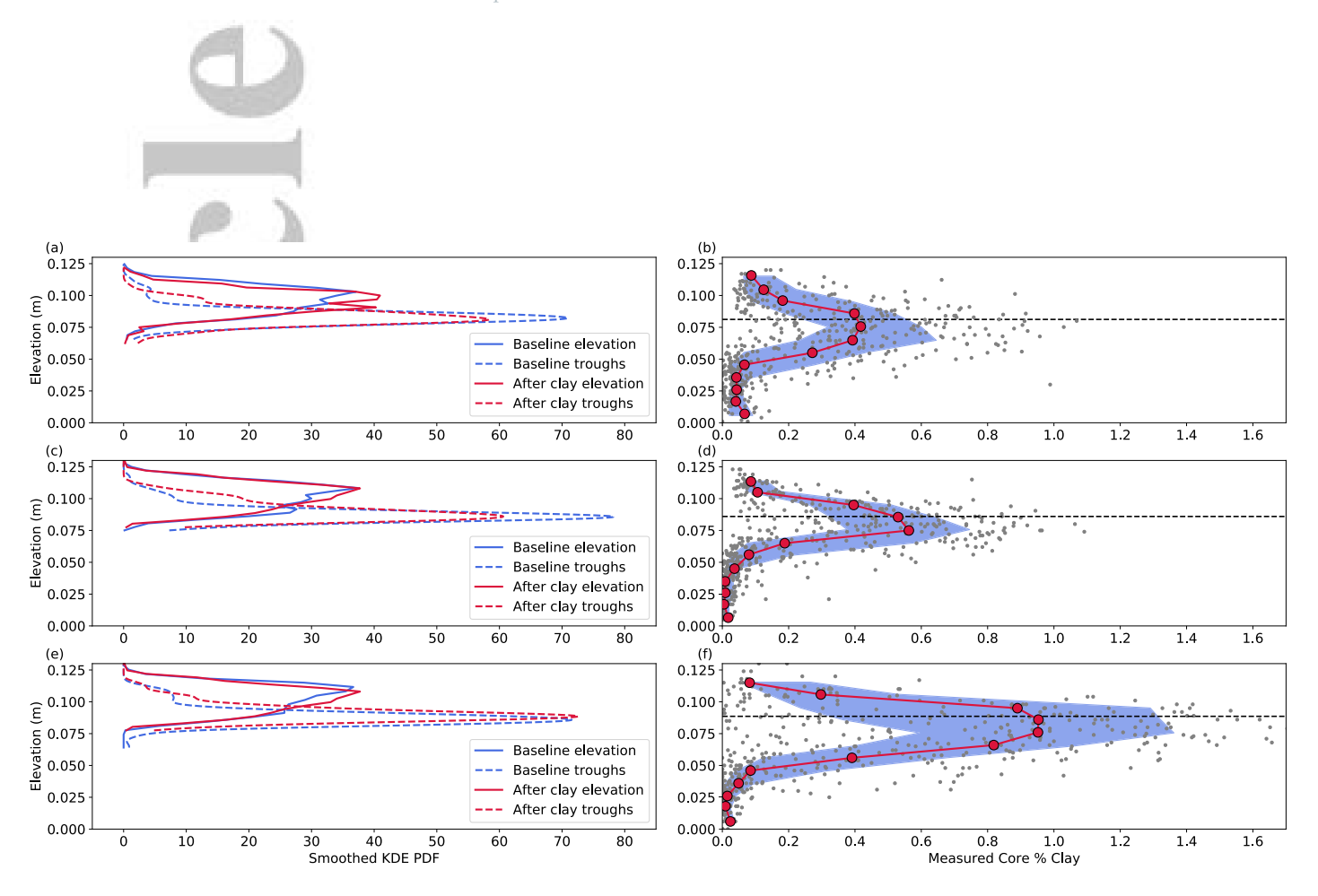


Figure 5. Visualization of bed and trough elevation kernal density estimations (KDE) and clay accumulation profiles for the sediment cores. Each row corresponds to an experimental run, with Runs 1, 2 and 3 shown on rows 1, 2 and 3 respectively. (a), (c) and (e) show bed elevation KDEs (solid lines) and trough elevation KDEs (dashed lines). Blue lines represent baseline measurements and red lines represent the final 96 hours of the experiment. (b), (d) and (f) show clay percentage as a function of depth for all cores. Grey dots are individual measurements while red dots represent the median over 1 cm of depth. The light blue shading represents the interquartile range (25/75 percentiles). The dashed black shows the location of most frequent scour after clay addition. The most frequent trough elevation is found just below the start of the clay layer. Due to a leak in the flume during Run 4, significant clay was pulled into the bed post experiment and disrupted the subsurface clay layer after the morphodynamic data was collected but before cores could be taken. Figure S4 contains the bed elevation and trough data for Run 4.

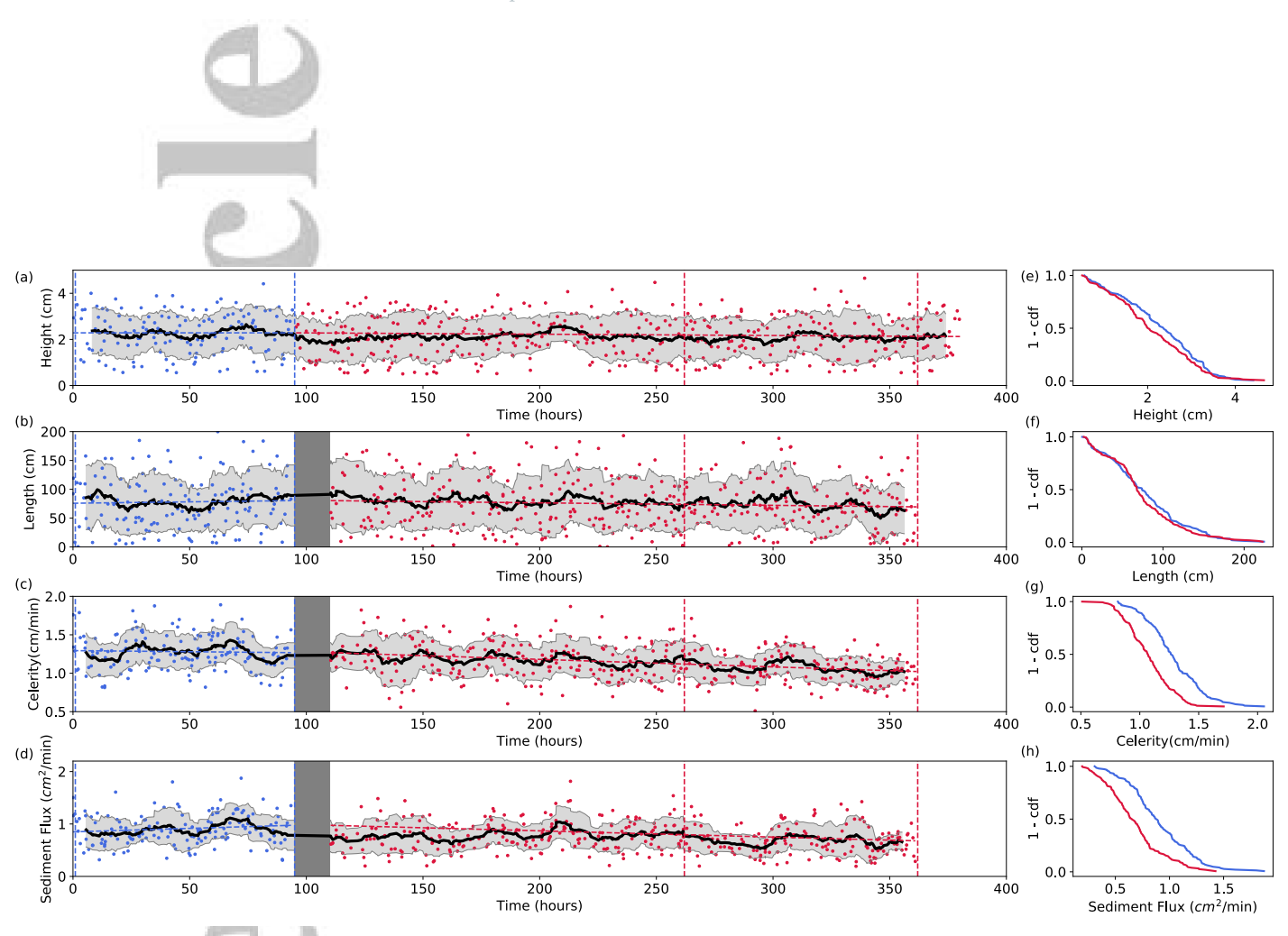


Figure 6. Time series and complimentary cumulative density functions (1-cdf) of height, length, celerity, and sediment flux for Run 1. Plots (a) and (e) show the timeseries and 1-cdf, respectively, for bedform height results. Length (b), (f) celerity (c), (g) - and sediment flux (d), (h) - are shown in successive rows. In the time series plots, the blue and red dots denote baseline and post-clay injection data, respectively. Solid black lines represent a rolling average of 20 hours while the light grey visualizes the standard deviation of this measurement. Solid grey rectangular boxes show missing data. Dashed vertical lines indicate the beginning and end of 96 hour data analysis windows, which are used in Tables 2 and 3. Additional dashed lines show linear fits to the data for the baseline window and the full post clay data-set. Plots of 1-cdf shown on the right are also based on these analysis windows where the blue and red lines represent the baseline and final measurement windows, respectively.

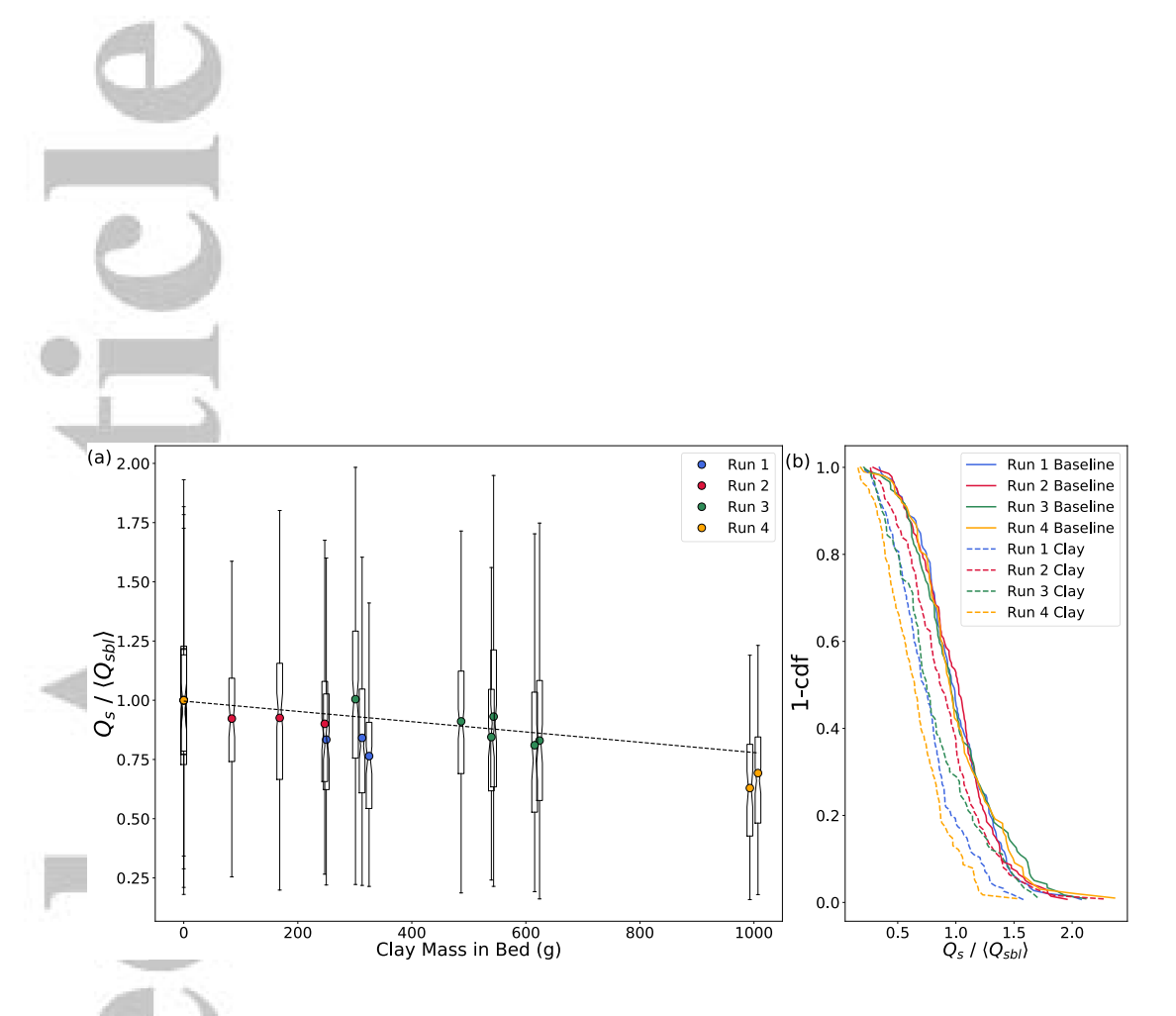


Figure 7. Variation in bedform sediment flux with increasing clay accumulation within the bed. (a) Box and whisker plots represent all bedform fluxes for a 100 hour window and the circles represent the mean values where the colors (red, blue, green, yellow) represent Runs 1-4, respectively. All data were normalized by the average value for that Run's baseline dataset for zero clay accumulation (denoted by the 'bl' subscript, see Table 2 for values). Box and whisker plot show variation inherent in each measurement window. The dashed line indicates a linear regression fit to all of the data. (b) 1-cdf for the baseline (solid lines) and final hundred hours (dashed lines) of the normalized sediment flux. Note that the 1-cdf shows decreasing flux with increasing clay accumulation for the entire population of measured bedforms.

A